Journal of Materials Processing Technology 147 (2004) 336–342

Journal of Materials Processing Technology

www.elsevier.com/locate/jmatprotec

Silicon nitride oxidation behaviour at 1000 and 1200 °C

Simone Pereira Taguchi*, Sebastião Ribeiro

Faculdade de Engenharia Química de Lorena—FAENQUIL-DEMAR, Polo Urbo Industrial, Gleba AI-6, s/n, cep 12600-000 Lorena, SP, Brazil

Received 20 March 2003; accepted 7 January 2004

Abstract

The oxidation behaviour of Si_3N_4–$Y_2Si_2O_7$ ceramics was investigated at 1000 and 1200 °C. These temperatures were chosen because most of the applications of Si_3N_4 occur at these temperatures. The Si_3N_4 samples were sintered by liquid phase sintering using 7 and 14 vol.% of $Y_2Si_2O_7$ as a sintering additive. The density of the sintered samples reached 99%. The samples were heated under stationary air for different periods of time between 0 and 256 h. The kinetic of oxidation was studied in function of the temperature and time of exposure, mainly during a short period of oxidation. The weight gain during the oxidative process reached values of 0.1 and 0.2 mg/cm^2 at 1000 and 1200 °C, respectively. The evolution of oxidised layers was analysed by X-ray diffraction (XRD) and scanning electron microscopy (SEM). The presence of β-Si_3N_4, γ-$Y_2Si_2O_7$, SiO_2 and Si_2N_2O phases was observed on the surface of samples by XRD. It was concluded that the Si_3N_4 shows a high oxidation resistance at 1000 and 1200 °C in atmospheric air, but special attention is required when the time of exposure is long, and temperature and the volume of additives is high.

Keywords: Sintering; Oxidation; Silicon nitride; Yttrium disilicate

1. Introduction

Silicon nitride has superior physical and mechanical properties compared to metals at elevated temperature [1,2]. The Si_3N_4 has a high thermal shock resistance due to its low thermal expansion coefficient and has good resistance to oxidation when compared to other structural materials. The positive Si_3N_4 properties allow the use of this structural material at high temperatures [2–5].

The covalent ceramics, such as Si_3N_4, do not produce high-density bodies by means of solid sintering because they have low auto-diffusion coefficients. In order to obtain high-density ceramics, liquid phase sintering must be used. Y_2O_3 additive sintering is normally used because it reacts with the SiO_2 layer covering the Si_3N_4 surface during the sintering, forming $Y_2Si_2O_7$. This compound is the most stable in the Y–Si–O system [6,7].

The Si_3N_4 oxidation depends on temperature, ceramic composition, atmosphere type, physical properties of the oxidation layer, additive composition and additive quantities. The possible chemical reactions [8] of Si_3N_4 oxidation systems, in air, are as follows:

$$Si_3N_4(s) + \tfrac{3}{4}O_2(g) \rightarrow \tfrac{3}{2}Si_2N_2O(s) + \tfrac{1}{2}N_2(g) \quad (1)$$

$$Si_3N_4(s) + \tfrac{3}{2}O_2(g) \rightarrow 3SiO(g) + 2N_2(g) \quad (2)$$

$$Si_3N_4(s) + 3O_2(g) \rightarrow 3SiO_2(s) + 2N_2(g) \quad (3)$$

$$Si_2N_2O(s) + \tfrac{3}{2}O_2(g) \rightarrow 2SiO_2(s) + N_2(g) \quad (4)$$

$$Si_2N_2O(s) + SiO_2(s) \rightarrow 3SiO(g) + 2N_2(g) \quad (5)$$

$$Si_3N_4(s) + SiO_2(s) \rightarrow 2Si_2N_2O(s) + N_2(g) \quad (6)$$

$$Si(s) + O_2(g) \rightarrow SiO_2(s) \quad (7)$$

The Gibbs free energy of formation ΔG°_f is lower for SiO_2, Si_2N_2O, and Si_3N_4, showing that the SiO_2 is thermodynamically more stable than the other species, as shown in Table 1. Du et al. [8] verified that the oxidation process of Si_3N_4 is limited by the reaction kinetics and not by the mass transport. The oxidation kinetic is influenced by intergranular phases that diffuse to the surface. Thermodynamic calculations estimate the probability for a reaction to occur for a given situation, but the kinetics remain very complex due to the diffusion mechanisms.

The cationic diffusion is easier than anionic diffusion because the metal ion is generally smaller than O^{2-} ion. When the ceramic is oxidising by cationic diffusion, a damage zone is formed on the ceramic–oxide interface. This phenomena

* Corresponding author. Tel.: +55-12-3159-9913; fax: +55-12-3153-3006.
E-mail address: simone@ppgem.faenquil.br (S.P. Taguchi).

0924-0136/$ – see front matter © 2004 Elsevier B.V. All rights reserved.
doi:10.1016/j.jmatprotec.2004.01.003

Table 1
Gibbs free energy of formation ΔG°_f of SiO_2(s), Si_2N_2O(s), and α-Si_3N_4(s) calculated at 1000 and 1200 °C

Species	ΔG°_f (kcal/mol) (25–1127 °C) [8]	ΔG°_f (kcal/mol) 1000 °C	ΔG°_f (kcal/mol) 1200 °C
SiO_2(s) amorphous	$-214.4 + 0.0406T$	−162.7	−154.6
Si_2N_2O(s) crystalline	$-223.7 + 0.0653T$	−140.6	−127.5
α-Si_3N_4(s)	$-176.9 + 0.0783T$	−77.2	−61.6

Table 2
Databases of Si_3N_4 compositions and weight change in different oxidation conditions

References	Additive	Temperature (°C)	Time (h)	Weight gain (mg/cm^2)
[6]	12 vol.% Y_2O_3/SiO_2 (forming $Si_3Y_2O_3N_4$)	1000	20	2.00
[6]	12 vol.% Y_2O_3/SiO_2 (forming $Y_2Si_2O_7$)	1375	303	0.21
[11]	14 vol.% Y_2O_3/SiO_2	1400	140	0.80
[11]	21 vol.% Y_2O_3/SiO_2	1400	64	0.80
[12]	CeO_2/Al_2O_3	1300	20	1.10
[12]	CeO_2/Al_2O_3	1400	20	2.23
[13]	11.89 vol.% Y_2O_3/AlN/SiO_2	1350	1	0.24
[13]	23.15 vol.% Y_2O_3/AlN/SiO_2	1350	1	0.86

accelerates the oxidation [9], which occurs in three stages: (i) oxygen adsorption on surface; (ii) oxide nucleation; (iii) growth of oxide layer.

The atoms in the surface of a crystal have fewer neighbours than the atoms in the bulk. Because of the tendency of surface atoms to saturate missing bonds, the surface atoms are highly reactive. This tendency depends on crystallographic orientation and also affects other properties such as the surface energy and the work function of the electrons. Asymmetrical forces on the surface atoms furthermore suggest that the topmost layer of atoms is displaced normally away from the next atomic layer. The adsorption is normally an exothermic process [10].

The oxidation product nucleates and grows laterally to produce a continuous film on the surface. The nucleation and growth of nuclei depend on the materials and their orientation, the temperature and the oxygen pressure. The nuclei growth is due to the adsorbed oxygen on the sample surface simultaneously causing oxygen depletion in zones around each nucleus and inhibiting the nuclei formation. The size of these zones, and thus the particle density, are governed by the supply of adsorbed oxygen (defined by oxygen pressure and temperature) and the rate of surface migration (defined by temperature and orientation). The nuclei formed near a large particle coalesce and contribute to the particle growth since the surface energy is lower for larger particles than for smaller ones [10].

The literature shows some databases [11–13] about Si_3N_4 oxidation in different test conditions (see Table 2). The objective of this work is to study the oxidation of Si_3N_4, in air, at temperatures used in several different applications.

2. Experimental procedure

The α-Si_3N_4 powder (SN-E10, Ube Industries Ltd., Japan) was mixed with 7 and 14 vol.% yttrium disilicate ($Y_2Si_2O_7$), called SNY7 and SNY14. The $Y_2Si_2O_7$ was produced by heat treatment at 1400 °C for 32 h, using SiO_2 and Y_2O_3 in 2:1 molar composition, respectively. The powder mixtures were milled in a planetary mill using isopropilic alcohol for 6 h. The slurries were vacuum dried at 80 °C. The dried powder was sieved and granulated through a 40 mesh sieve before forming by uniaxial pressure at 30 MPa and cold isostatic pressure at 300 MPa.

Sintering was performed in a graphite resistance heated furnace (Thermal Technology 1000-4560-FP20) with the samples placed in a powder bed (60 wt.% Si_3N_4, 30 wt.% BN, and 10 wt.% SiO_2), using a heating rate of 20 °C/min, up to 1800 °C, in a nitrogen atmosphere of 1.8 MPa. The isotherm sintering was 4 h long. The surfaces of samples were ground and polished to 3 μm finishing. Prior to oxidation, the surfaces were ultrasonically cleaned in acetone and dried at 100 °C. The density was measured by a geometrical method, and the porosity was analysed by Hg porosimetry using 0.29–227.53 MPa pressure, corresponding to pores diameter, ranging from 5 to 64×10^{-4} μm. The oxidation test conditions are shown in Table 3.

After the oxidation test, the weight gain was determined as a function of time and the products were analysed by XRD method, using JCPDS comparison, for all times and temperatures of oxidation. The microstructures of samples were analysed using SEM/EDS.

Table 3
Oxidation test conditions

Test temperature (°C)	Exposure time (h)
1000	0, 0.5, 1, 2, 4, 8, 16, 32, 64, 128, and 256
1200	0, 0.5, 1, 2, 4, 8, 16, 32, 64, 128, and 256

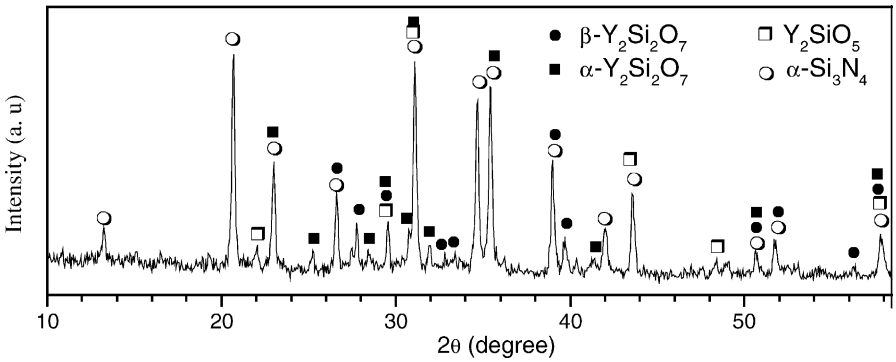

Fig. 1. Powder XRD patterns for α-Si_3N_4/$Y_2Si_2O_7$ mixture.

3. Results and discussion

3.1. Characterisation of samples before oxidation

The α-Si_3N_4 and $Y_2Si_2O_7$ phases of the pressed samples were analysed by XRD, as shown in Fig. 1. During the sintering, the samples showed the transformation $\alpha \rightarrow \beta$ Si_3N_4 and density of $99.01 \pm 1.09\%$.

The sintered samples also showed the presence of a Si_2N_2O phase (Fig. 2). The Si_2N_2O phase appeared due to the reaction between SiO_2 (powder bed composition or surface of Si_3N_4 powder, as shown in Eq. (6)) and Si_3N_4. After sintering, the secondary phase, $Y_2Si_2O_7$, is amorphous. The absence of pores was confirmed by a porosity test, showing the good quality of the samples for the oxidation tests.

3.2. Phases on the oxidised surfaces

The oxidised layers at 1000 and 1200 °C showed the predominant presence of β-Si_3N_4 when compared to γ-$Y_2Si_2O_7$ phases. Fig. 3 shows the behaviour of SiO_2 and $Y_2Si_2O_7$ phases with exposure time at 1200 °C. The crystallisation and migration toward surface of the secondary phase started during the heating time for samples exposed at 1000 °C and after 0.5 h for samples exposed at 1200 °C. The quantities of crystallised secondary phase are higher for 1200 °C than for 1000 °C. The crystallisation and migration depends on the time and the temperature. The migration occurs later than the crystallisation because the migration depends on the SiO_2 formation (as shown in Eq. (3)). The $Y_2Si_2O_7$ is stable in Si_3N_4, but it migrates to the surface when oxidation of Si_3N_4 occurs. The SiO_2 formation on the surface produces a compositional gradient in the sample, and this gradient is the driving force to additive migration. Crystoballite phase, SiO_2, appeared after 8 h of exposure only for sample SNY7 at 1200 °C, and after 2 h of exposure for SNY14 samples. The Si_2N_2O appeared as a minor phase. Some authors agree upon the Si_2N_2O appearance on the oxidised samples [8,14,15], and affirm that this phase can delay the oxidation process. But other authors do not believe in the Si_2N_2O thermodynamic stability [11]. The Si_2N_2O can be amorphous depending on the process conditions, but the majority of the oxidation layer is SiO_2.

Fig. 4 shows the clear and dark regions of the oxidised surface, obtained by SEM. In the clear regions Si, O and Y can be identified by EDS analysis. In the dark regions Si, O and N can be identified corresponding to Si_3N_4, SiO_2, or Si_2N_2O phases.

3.3. Weight change of samples during oxidation time

Fig. 5 shows the weight change of samples at 1000 and 1200 °C up to 256 h of exposure in air. The SNY7 and SNY14 samples presented small weight changes, e.g. do not

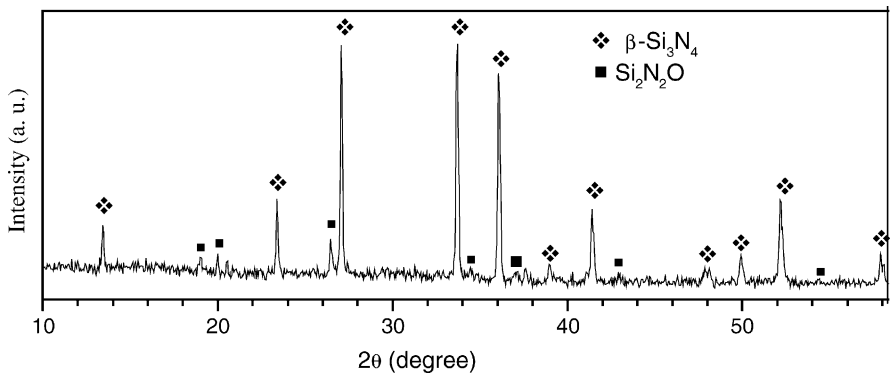

Fig. 2. XRD patterns of Si_3N_4 sintered ceramic.

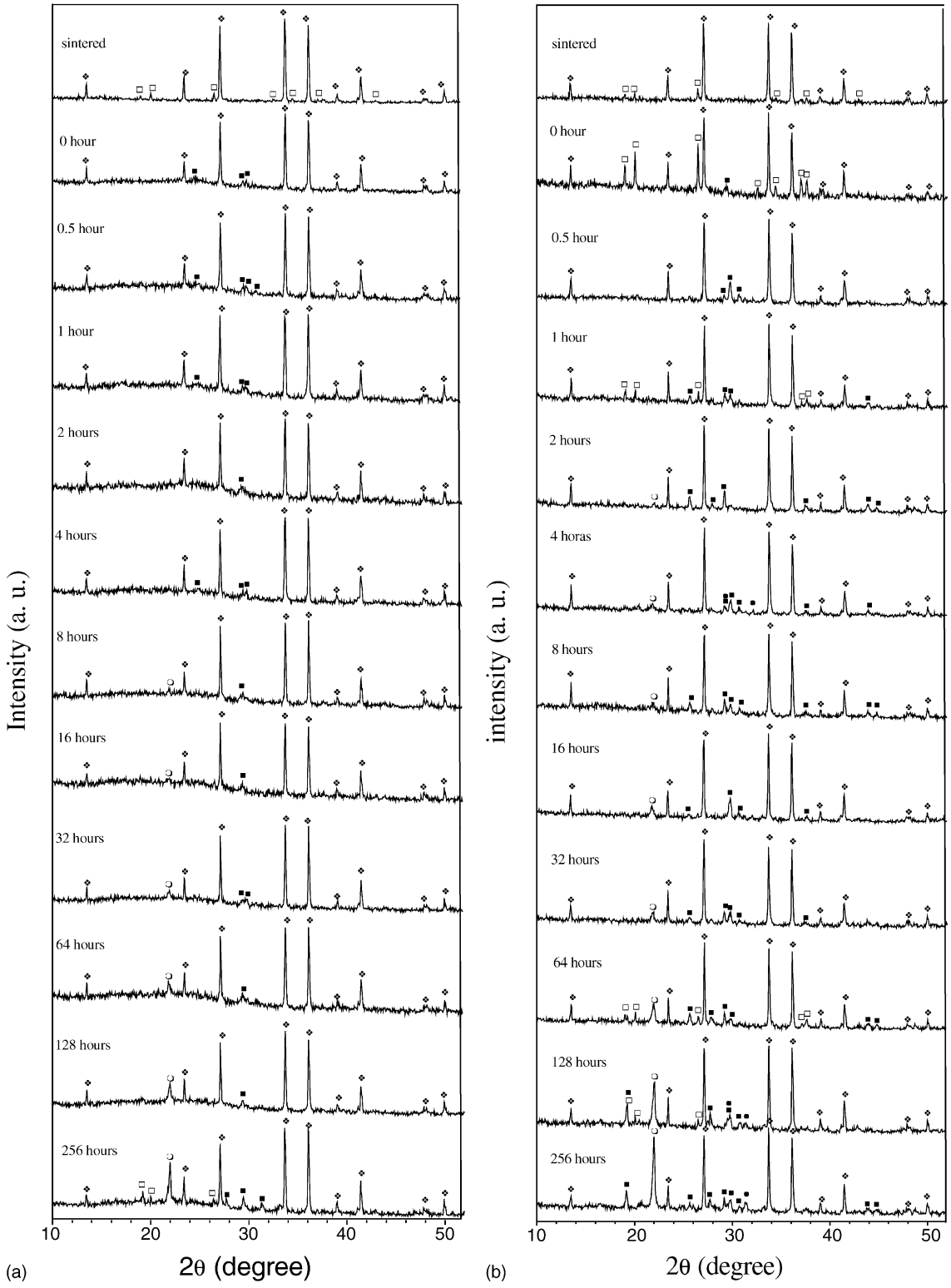

Fig. 3. X-ray diffraction of (a) SNY7 and (b) SNY14 oxidised at 1200 °C.

oxidise at 1000 °C. The weight change at 1200 °C was twice the value at 1000 °C, reaching 0.2 mg/cm^2, and the rate of oxidation was higher after 128 h of exposure, indicating the possible change in the oxidation mechanism.

When the oxidation product has been nucleated, during the initial exposition time, its quantity is insignificant and allows easy adsorption of oxygen on the surface. This oxidation continues until all surface is covered by the product

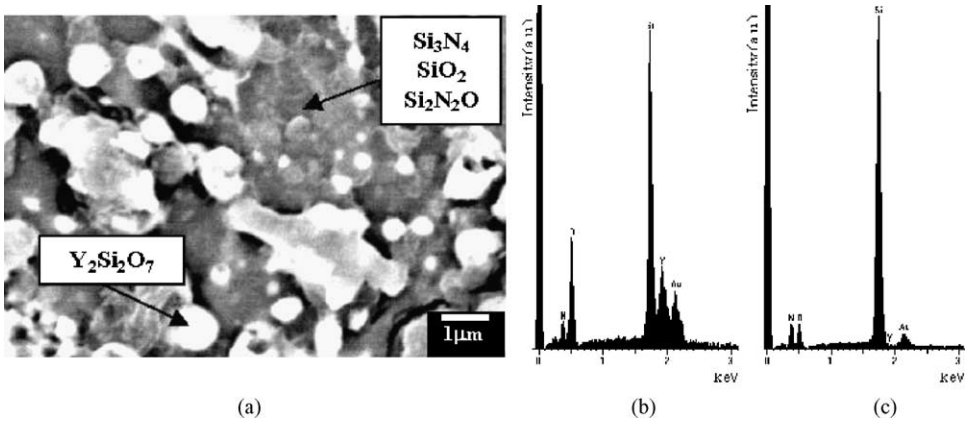

Fig. 4. (a) SEM micrograph using backscattered electrons; (b) EDS spectra of clear regions on surface; (c) EDS spectra of dark regions on surface.

of oxidation and, after this, the oxidised layer hinders the oxygen diffusion to the bulk and the oxidation rate reduces.

The time and temperature are very important for the oxidation of Si_3N_4 ceramics. The crystoballite formed by reaction unbalanced the sample composition gradient. For this reason, the $Y_2Si_2O_7$ migrates to the surface and the oxidation was accelerated. The results of X-ray diffraction showed the increase of SiO_2 and $Y_2Si_2O_7$ quantities on the surface of samples oxidised at 256 h of exposure at 1200 °C following the results of weight change. Samples with more quantities of the secondary phase presented higher weight changes with time, and this is intensified also by temperature increase (as showed in Fig. 5).

This work showed lower or equivalent values for weight change than the literature, though the conditions of the system are different (Table 2). This comparative analysis with literature is only a simple reference; considering there is no classification table for oxidation resistance, like that for metals.

3.4. Interface and surface microstructures of oxidised samples

Fig. 6 shows the section of samples SNY7 and SNY14 exposed for 256 h at 1000 and 1200 °C. Sample SNY7 exposed at 1000 °C presented a fine layer of SiO_2, as well as a change in microstructure and microcracks near Si_3N_4/SiO_2 interface, probably due to the additive migration to the surface and the N_2 production by oxidation reactions (Eqs. (1)–(6)). This behaviour is intensified by temperature, time and composition increase (as showed in Fig. 6(b)–(d)). The oxidised layer of the SNY7 sample is more adherent than SNY14 because it has lower intergranular phase quantities in the sample, and this leads to a lower cation migration to the surface and to a lower oxidation rate. The crystoballite thermal expansivity changed from 0.2 to 1.6% around 250 °C. The Si_3N_4 expansivity does not have this abrupt change. The Si_3N_4 expansivity grows slowly until 0.44% at 1200 °C. During the cooling, compressive and tensile forces are

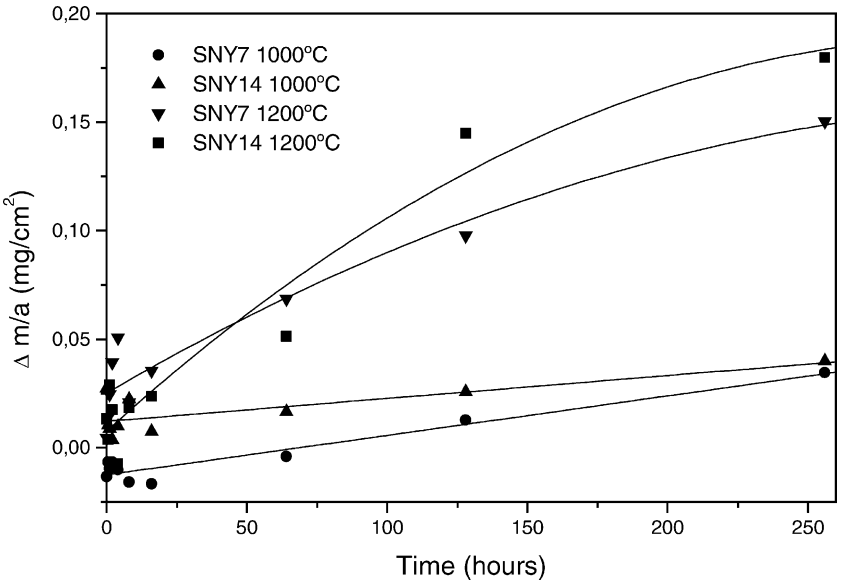

Fig. 5. Weight change of SNY7 and SNY14 samples at 1000 and 1200 °C.

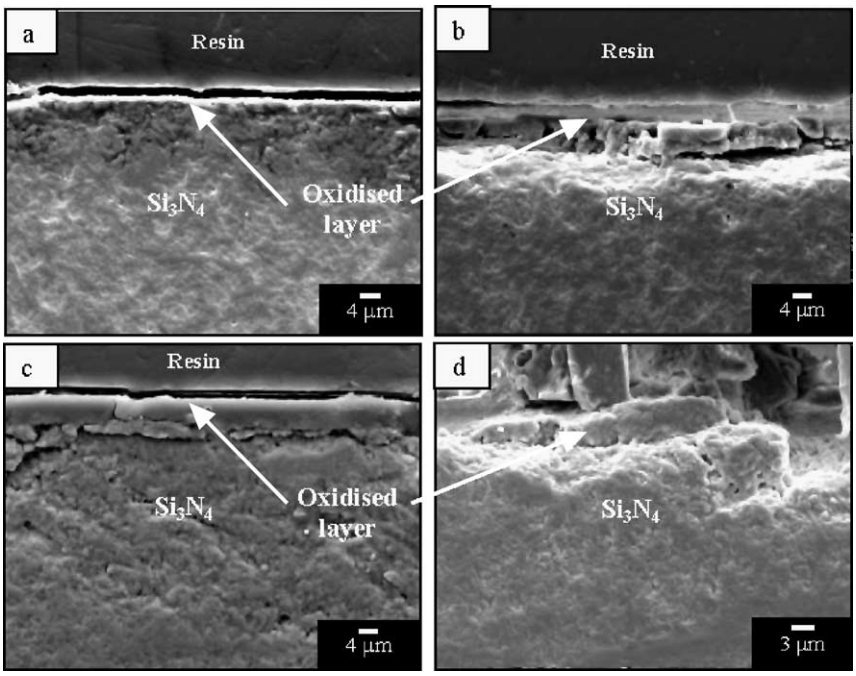

Fig. 6. SEM micrograph of sample sections exposed for 256 h: (a) 1000 °C (SNY7); (b) 1200 °C (SNY7); (c) 1000 °C (SNY14); (d) 1200 °C (SNY14).

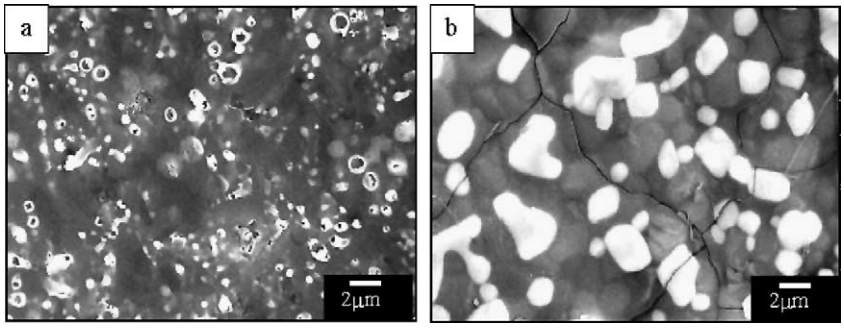

Fig. 7. Microstructure obtained by SEM of SNY14 surfaces oxidised at 1200 °C (a) for 1 h and (b) for 256 h of exposure in air.

produced on the Si_3N_4/SiO_2 interface [16]. These forces promote the formation of microcracks in crystoballite layer. Probably, this microcrack formation is due to the differential thermal expansion between Si_3N_4 and SiO_2. These microcracks can be seen in Figs. 6 and 7.

Fig. 7 shows the microstructure of SNY14 surfaces exposed at 1 and 256 h at 1200 °C. All SNY7 and SNY14 samples oxidised at 1000 °C exhibited the same microstructure as shown in Fig. 7(a). SNY14 samples oxidised for 64 h at 1200 °C exhibited the microstructure as shown in Fig. 7(b).

4. Conclusions

The results with both compositions of Si_3N_4 ceramics showed that they can be used at 1000 °C without an adverse effect on oxidation resistance. Applications at 1200 °C during long periods of exposure must receive a careful analysis due to the significant increase of oxidation rate with time. The additive quantity has a significant influence on Si_3N_4 oxidation. More additive quantities promote a higher oxidation rate.

It can be concluded that these ceramics have good oxidation resistance, but for long exposure times, high temperatures and high composition of additives they should be used with due care.

Acknowledgements

We gratefully acknowledge the financial support from CAPES—Brazil.

References

[1] L. Chuck, S.M. Goodrich, N.L. Hecht, D.E. McCullum, High-temperature tensile strength and tensile stress rupture behavior of Norton/TRW NT-154 silicon nitride, Ceram. Eng. Sci. Proc. 11 (7/8) (1990) 1007–1027.

[2] W. Dressler, R. Riedel, Int. J. Refract. Met. Hard Mater. 15 (1–3) (1997) 13–47.
[3] H. Huang, L. Yin, L. Zhou, High speed grinding of silicon nitride with resin bond diamond wheels, J. Mater. Proc. Technol. 141 (2003) 329–336.
[4] T. Otani, M. Hirata, High rate deposition of silicon nitride films by APCVD, Thin Solid Films 442 (2003) 44–47.
[5] S. Ogata, N. Hirosaki, C. Kocer, Y. Shibutani, A comparative ab initio study of the "ideal" strength of single crystal α- and β-Si_3N_4, Acta Materialia 52 (2004) 233–238.
[6] F.F. Lange, S.C. Singhal, R.C. Kuznicki, Phase relations and stability studies in the Si_3N_4–SiO_2–Y_2O_3 pseudoternary system, J. Am. Ceram. Soc. 60 (1977) 249–252.
[7] M.K. Cinibulk, G. Thomas, Oxidation behavior of rare-earth disilicate-silicon nitride ceramics, J. Am. Ceram. Soc. 75 (1992) 2044–2049.
[8] H. Du, R.E. Tressler, K.E. Spear, Thermodynamics of the Si–N–O system and kinetic modeling of oxidation of Si_3N_4, J. Electrochem. Soc. 136 (1989) 3210–3215.
[9] V. Gentil, Corrosão, Editora Guanabara Dois S. A., 3rd ed., Rio de Janeiro, 1996, pp. 117–124.
[10] P. Kofstad, High Temperature Corrosion. Elsevier, London/New York, 1988, p. 558.
[11] X. Pan, Atomistic structure of silicon nitride/silicate glass interfaces, J. Am. Ceram. Soc. 79 (1996) 2975–2979.
[12] J. Echeberria, F. Castro, Oxidation of silicon nitride sintered with ceria and alumina, Mater. Sci. Technol. 6 (1990) 497–503.
[13] S.K. Biswas, J. Mukerji, P.K. Das, Oxidation of silicon nitride sintered with yttria and magnesia containing nitrogen rich liquid, Eng. Mater. 89–91 (1994) 271–274.
[14] N.S. Jacobson, Corrosion of silicon-based ceramics in combustion environments, J. Am. Ceram. Soc. 76 (1993) 3–28.
[15] J. Chen, Oxidation of pure Si_3N_4: spectroscopic ellipsometry and glancing angle X-ray diffraction studies, Eng. Mater. 89–91 (1994) 301–306.
[16] D.A. Colling, T. Vasilos, Industrial Materials, vol. 2. Prentice-Hall, Englewood Cliffs, NJ, 1995, p. 233.